Ultrasonics Sonochemistry 85 (2022) 105982

Contents lists available at ScienceDirect

Ultrasonics Sonochemistry

journal homepage: www.elsevier.com/locate/ultson

A novel sub-pilot-scale direct-contact ultrasonic dehydration technology for sustainable production of distillers dried grains (DDG)

Amir Malvandi [a], Danielle Nicole Coleman [b], Juan J. Loor [b], Hao Feng [a,c,*]

[a] Department of Agricultural and Biological Engineering, University of Illinois at Urbana- Champaign, Urbana, IL, 61801, USA
[b] Department of Animal Sciences and Division of Nutritional Sciences, University of Illinois at Urbana-Champaign, Urbana, IL, 61801, USA
[c] Department of Food Science and Human Nutrition, University of Illinois at Urbana-Champaign, Urbana, IL, 61801, USA

ARTICLE INFO

Keywords:
Non-thermal drying
Modulated ultrasound
dried distillers grains (DDG)
Acid detergent insoluble crude protein
Process enhancement

ABSTRACT

DDG is a major source of protein, calcium, phosphorus, and sulfur is arguably the most important byproduct of the bioethanol industry with increasing demand over the past few years. Reducing energy consumption in the DDG production process and energy recovery from DDG is vital for sustainable bioethanol productions. In this paper, a novel direct-contact multi-frequency, multimode, and modulated (MMM) ultrasonic dryer (US) was developed for the first time and has been applied in dehydration of wet distillers' grain (WDG). Ultrasonic drying (US) was combined with a convective airflow (HA) at different temperatures of 25 (room temperature), 50 and 70 °C to evaluate the impact of US, HA, and US + HA on drying kinetics, activation energy, chemical compositions, microstructure, and color of DDG. Semi-empirical kinetic models were developed and evaluating drying performances showed that the application of ultrasound significantly enhanced the drying rate and decreased the drying time (by 46%), especially at low drying temperatures. The activation energy for moisture removal in the presence of ultrasound was about 50% of that without ultrasound. The final dried distillers' grains product processed by ultrasonic drying had a brighter color, a higher available protein, a higher digestible protein (the lowest acid detergent insoluble crude protein), and a better surface profile with no compromise on minerals and fiber contents.

1. Introduction

Biofuels are the fourth leading renewable energy resource after hydro, wind, and solar, and are widely used in the United States in the form of bioethanol-gasoline (E5) fuel blends. Using ethanol reduces crude oil imports, air pollution, carbon footprints, and greenhouse gases. According to the U.S. Energy Information Administration (EIA), fuel ethanol production capacity in the United States is 17.3 billion gallons per year (gal/y). In 2020, the United States, with a global market share of 53% and annual production of over 13.9 billion gallons, remained to be the world's largest producer of ethanol. The corn dry grind process is responsible for 90% of bioethanol production in the US, and it also produces valuable co-products [1].

Dried and wet distiller's grain (DDG and WDG) are major byproducts of bioethanol production, in both size and value. With approximately 2.7 gallons of ethanol from one bushel of corn (~25.4 kg), 8.16 kg of DDG will be produced [2]. These byproducts are renewable and sustainable resources containing a large amount of protein, oil, energy, and fiber [3–4]. The digestible phosphorous content in DDG makes it an excellent replacement for conventional feed ingredients such as corn and soybean meals [5]. WDG and DDG help offset the low ethanol prices and are a major support for agricultural output and farm income, support the social fabric of our rural communities, and promote a sustainable agricultural system.

While WDG can be sold locally to cattle feeders, its high moisture content (around 70%) precludes it for long-distance transportation. Problems such as caking during transportation and storage, microbial spoilage, shelf life, and flowability are the major driving forces for drying of WDG (and mixing with condensed distillers' solubles) to obtain distiller's dried grain (DDG) with 88% dry matter and long shelf life [6]. The nutrient profile of DDG depends not only on its source, as a wide variety of feedstocks with different nutrient compositions is used for producing ethanol, but also on processing factors like drying, fermentation, and grind procedure [7–9]. Current DDG drying methods involve the use of high temperatures. In the high-temperature drying processes, heat damage due to a chemical reaction, known as the

* Corresponding author at: Department of Agricultural and Biological Engineering, University of Illinois Urbana-Champaign, USA.
E-mail address: haofeng@illinois.edu (H. Feng).

https://doi.org/10.1016/j.ultsonch.2022.105982
Received 11 November 2021; Received in revised form 1 March 2022; Accepted 12 March 2022
Available online 17 March 2022

Fig. 1. Schematic of MMM ultrasonic contact dryer.

Maillard reaction, plays an important role [10]. Several studies have examined the effect of drying on the loss of nutrients in the DDG. Tang et al. [11] used superheated steam to dry thin layer spent grains and concluded that increasing steam temperature and velocity enhanced drying rate but it gelatinized more starch and decreased the starch content. Digestibility and available protein, because of their vulnerability to heat damage, are one of the major concerns of using DDG as a feed component for monogastric animals [12]. Plant scale experiments were conducted by Kingsly et al. [13] and Clementson and Ileleji [14] on corn DDG to evaluate the effects of adding condensed distillers soluble to WDG on the chemical and physical composition of the final product. Bhadra et al. [15] argued that increasing drying temperature resulted in greater denaturing of protein and less protein dispersibility index. Mosqueda et al. [16] evaluated the protein quality of wheat DDG dried by different drying technologies including forced air convection, microwave, and microwave–convection methods by monitoring acid detergent insoluble crude protein (ADICP) and lysine content. They concluded that microwave and microwave-assisted drying decreased the operating temperature and shorten the exposure times, thereby improving the protein quality of DDG. Other researchers also stated that the high temperature and drying time could have a detrimental impact on the feeding value of distillers grains (by reducing the availability and digestibility of protein) [12,17–18]. In addition, the higher the drying temperature, the higher the utility and maintenance costs in bioethanol plants [15], the higher volatile organic compounds (VOC) emissions, the higher fire or explosion risk, the higher irreversibility, and less sustainability. The most prevalent dryer styles of producing DDG are rotary drum dryers and ring dryers which are usually operated at excessive temperatures and are quite energy-intensive, which are estimated to account for about one-third of the whole energy consumption of ethanol plants [19]. Therefore, there is a need to reduce the drying temperature of industrial dryers in bioethanol plants. However, reducing temperature usually follows with an increase in the drying time in almost all conventional thermal dryers. Thus, innovative effort into the development of new drying concepts that can reduce both the drying time and temperature would be of great interest.

The use of ultrasonic energy, which is considered as one of the non-thermal processing methods, for drying of heat-sensitive materials such as foods has drawn increasing attention in recent years [20–21]. Airborne ultrasound was typically applied in previous studies and enhancement in heat and mass transfer rates over the surface of products was reported [22]. However, the large impedance mismatch between air, transducer, and the product, decreases the energy efficiency of airborne ultrasonic dryers so they have not found their path to commercial applications. Recently, ultrasonic direct contract drying has been developed by a few researchers to overcome the impedance mismatch issue and improve the efficiency of the system [23–26]. In ultrasonic direct contacting drying, extraction of water by mechanical vibration at a frequency of 20 kHz and above was reported to reduce the drying time and temperature simultaneously. In addition, lower energy consumption was reported as a result of water removal in the form of misting without a phase change when free water was abundant. Similar to microwaves, however, ultrasonic pressure distribution on the drying surface that is vibrated by ultrasound is not uniform. This calls for the development of a new strategy to ensure uniformity of the ultrasonic field on the drying surface.

This study reported the first attempt to develop a novel sub-pilot multi-frequency, multimode, and modulated (MMM) ultrasonic dryer and used to produce DDG with improved nutrient quality. This unique direct-contact MMM ultrasonic system can provide a uniform, repeatable, and homogenous distribution of high intensity vibrations on the drying surface while avoiding the creation of stationary/standing waves by synchronously excite multiple vibrating modes on a surface [27]. Such feature is ideal and crucial for drying system to provide a more uniform product. In addition, this unique ultrasonic system can operate under non-thermal conditions (25 °C) to perform drying and can decrease the drying time simultaneously. The drying kinetics and quality attributes of the DDG, including color, crude protein, amino acids, minerals, fibers, and microstructures were investigated, in comparison with that dried by freeze drying. The effect of hot air in combination with ultrasonic drying was also evaluated. To the best of the authors' knowledge, no study has thus far been communicated on the application of ultrasonic energy in the drying of DDG.

2. Materials and methods

2.1. Experimental setup

Fig. 1 shows the experimental setup which consists of an MMM ultrasonic module, a close-loop drying chamber with a rectangular cross-section, temperature and airspeed sensors, an air blower, and an air heater. Airflow was generated by a centrifugal blower (Dayton, Model 1C791) driven by a belt-drive motor (Dayton, single-speed, 1725 RPM). The incoming air temperature to the ultrasonic module was adjusted by a heater controlled by a digital dual NTC temperature controller (STC-3008, Walfront), with an accuracy of ± 1 °C and resolution of 0.1 °C. The air was used to remove moisture from the sample, and also provide an option for hot-air and ultrasound combined drying. An airspeed sensor was used to monitor the airspeed inside the channel (Matek, Digital Airspeed Sensor ASPD-4525). The MMM ultrasound module consisted of an ultrasonic generator that produced a sweeping frequency and adaptively modulated waveform with a maximum power of 1,000 W, b) a piezoelectric transducer at 20 kHz, c) an acoustical wave-guide that connected the acoustic load to the transducer, and d) acoustic sensors adjacent to the waveguide to create regulation feedback between acoustical load and power supply. The MMM ultrasonic system created a strong and uniform vibration on the metallic drying surface onto which the wet samples were placed. The MMM module uses digital signal processing to synchronously excite a large number of vibrating modes including harmonics and sub-harmonics of acoustic loads to create a uniform vibration over the surface [27]. Finally, compressed air was used to cool down the piezoelectric transducer of the MMM system.

2.2. Sample preparation and experimental procedure

Wet distillers grain (WDG) was received from Flint Hills Resources, LLC in frozen form and kept in a cold room at −40 °C. The WDG was a mechanically separated high protein distillers' grain produced from corn in a dry mill ethanol plant. Prior to each experiment, the samples were thawed by placing them at room temperature for 24 h. The initial moisture content of the WDG was measured for each batch of samples and was around 76% (wet basis). Ultrasound was set to the maximum power of 200 W and the generator excited the vibrating sheet with a central frequency of 20 kHz and a sweeping frequency of 1 kHz. The sweep range was determined with an adaptive control system in real-time and dynamically to avoid the formation of stationary or standing waves that generate regions of high and low acoustic activity (which typically produced by traditional ultrasonic systems operating at a single frequency). In addition, to avoid the overheating of the piezoelectric transducer as well as reducing the energy consumption, ultrasound was operated in pulsed mode (on/off mode). The operation time where the ultrasound was on, known as pulse length, was set to 5 s and the non-operation time, known as interval length, was set to 1 s. To remove the mist produced by ultrasonic vibration, a uniform airflow was allowed to pass over the samples. Three air temperature settings were used for the airflow: 25 °C, 50 °C, and 70 °C. The airspeed was constant and the average value over the samples was 1.5 m/s. Three sets of experiments were conducted: ultrasound alone (US), hot air alone (HA), and US + HA. All the settings were adjusted well before placing the samples inside the dryer to make sure that the fully hydrodynamic and thermally steady-state conditions have reached. Then, about 100 g of WDG samples were spread onto the surface of the ultrasonic vibrating surface using a hand roller into a uniform thickness of 2 mm. A cork borer was used to divide the samples into a series of small circular subsamples with a diameter of 15 mm. At each time step, circular samples were picked randomly from the dryer and weighted by a digital balance with an accuracy of ± 0.0001 g (Ohaus Corp., 166AP110S, Switzerland) to record the weight loss over time. Changes in the weight of DDG samples were recorded and used to find the wet basis moisture content and the drying rate. After weighting, the samples were transferred to an aluminum pan, which was placed in a convection oven (Thermo Scientific Precision™ Compact Oven) (105 °C) for 3 h to remove the remaining moisture and find the solid content (NFTA Method 2.2.2.5) [28]. The drying process was continued until the sample weight change became negligible. For freeze-drying (FD), the fresh WDG samples were spread into a thin layer of 2 mm thick and frozen instantly with liquid nitrogen before putting in a cold room at −40 °C for 48 h. Then, they were placed inside the freeze-drying chamber (Harvest Right Inc., Utah, USA) and FD was performed by setting the heating plate temperature at 46 °C under a vacuum of 140–150 mTorr.

The final equilibrium moisture content for freeze dried product was in the range of 2–3% wet basis moisture content. For hot air and ultrasonic dried products, the final moisture was in range of 7–8% in wet basis. Dried samples then were placed in resealable Mylar bags filled with nitrogen gas to have a perfect storage condition.

2.3. Determination of drying variables

At time t, the wet basis (wb) and dry basis (db) moisture contents were calculated and the drying rate DR (min^{-1}) was determined via.

$$DR(t) = \frac{M_{db}|_t - M_{db}|_{t+\Delta t}}{\Delta t} \tag{1}$$

The moisture ratio (MR) during drying can be obtained using.

$$MR(t) = \frac{M_{db}(t) - M_{eq}}{M_i - M_{eq}} \tag{2}$$

where subscripts eq and i represent the equilibrium and initial conditions, respectively. MR is an important non-dimensional variable for developing drying models and describing drying kinetics. (1-MR) describes the water removed with regard to the total available water, thereby signifying the speed of drying. MR has a normalizing effect on the drying curves which is a necessity to formulate general drying models.

2.4. Effective moisture diffusivity and semi-empirical drying models

Drying kinetics are complex and have important effects on the quality of the final product. Thus, it is consequential to develop mathematical models to simulate drying at various conditions. Although there are different stages and mechanisms in the drying profile (initial stage, constant-rate period, and falling rate period), it is a common consensus to consider the falling rate period as the dominant process and use unsteady one-dimensional Fick's 2nd law of diffusion for an infinite slab geometry to describe the moisture gradient for a thin layer drying process as follows [29].

$$\frac{\partial X}{\partial t} = D_{eff}\frac{\partial^2 X}{\partial y^2} \tag{3}$$

where X is local dry basis moisture content, t (s) is drying time, and D_{eff} ($m^2 s^{-1}$) is effective moisture diffusivity. Eq. (3) assumes that D_{eff} is independent of local moisture content. However, it is a function of total moisture content and varies during drying. A simple solution of Eq. (3) is typically subjected to the following assumptions and conditions; a) a uniform initial moisture distribution inside the material, b) negligible shrinkage, and c) surface of the material is in thermal equilibrium with the surrounding air. Thus, an analytical solution of Eq. (3) for a slab geometry can be obtained via Crank [30]:

$$MR = \frac{8}{\pi^2}\sum_{n=1}^{\infty}\frac{1}{(2n-1)^2} exp\left[-\frac{(2n-1)^2\pi^2 D_{eff} t}{(2L)^2}\right] \tag{4}$$

where $L(m)$ is the half sample thickness. This solution assumes that the external mass transfer resistance is negligible, and the internal diffusion is the dominant mechanism controlling the drying process. Many studies

Table 1
Different semi-empirical drying models used for fitting experimental data.

Model Name	Equations	Constants
Lewis model [34]	$MR = exp(-kt)$	k
Page model [35]	$MR = exp(-kt^n)$	k, n
Henderson and Pabis model [36]	$MR = aexp(-kt)$	k, a
Logarithmic model [37]	$MR = aexp(-kt) + b$	k, a, b
Two-term model [38]	$MR = aexp(-kt) + bexp(-mt)$	k, a, b, m
Midilli model [39]	$MR = aexp(-kt^n) + bt$	k, n, a, b

used the leading term in the series solution of Eq. (4) to evaluate the effective moisture diffusivity during drying which imposes a constant effective diffusivity during drying. However, the nonlinear dependence of effective diffusivity to moisture content, particularly at the initial stages of drying is well-documented [31–32]. Here, Maple software[33] was used to expand Eq. (4) to several terms, and the effective moisture diffusivity was obtained by fitting the experimental data. By trial and error, a sufficient number of terms was selected at each time step to minimize the truncation error in evaluating effective diffusivity.

Semi-empirical drying models have been used for cost-effective prediction of the drying kinetics and control of the drying process [40]. These models are either based on simplifying Fick's second law or by incorporating physics into the empirical equations. Like empirical models, semi-empirical models do not involve any assumption on geometry, mass diffusivity, or conductivity and only require a small amount of computing time compared to the multiphase/multiphysics theoretical models. Here, six different drying models, as detailed in Table 1, were considered to fit the thin layer drying experimental data. Levenberg–Marquardt algorithm (LMA) [41]was used to find the unknown constants of models via solving nonlinear least square problem arises in curve-fitting. The goodness of fitting was evaluated using the coefficient of correlation (R^2), reduced chi-square (χ^2), and residual sum of squares (RSS) which are defined as:

$$RSS = \sum_{i=1}^{N} \left(MR_{measured}(i) - MR_{predicted}(i)\right)^2$$
$$R^2 = 1 - \frac{RSS}{\sum_{i=1}^{N} \left(\overline{MR_{measured}(i)} - MR_{predicted}(i)\right)^2} \quad (5)$$
$$\chi^2 = \frac{\sum_{i=1}^{N} \left(MR_{measured}(i) - MR_{predicted}(i)\right)^2}{N - n_0}$$

where n_0 and N represent the number of constants (in the model) and observations, respectively. R^2 represents the level of agreement among predicted and measured values and ranges from 0 to 1. The closer it is to 1, the greater the relationship exists between the predicted and experimental values. χ^2 and RSS signify how close are the predicted values to the experimental measurements and minimizing them lead to a model with great prediction capability.

2.5. Activation energy

The amount of energy required to remove moisture from a material depends on material-moisture binding. Different types of energies are associated with moisture-binding, including chemically bound moisture (5 kJ/mol), physicochemical bound moisture (3 kJ/mol), and physicomechanical binding (0.1 kJ/mol) as given in the literature [42]. Thus, the energy required for removing moisture depends not only on the solid matrix but also on the drying technology that determines the mechanism of removing moisture. Arrhenius equation is generally used to describe the relationship among the effective moisture diffusivity, activation energy, and temperature [43]. Arrhenius equation can be written as.

$$D_{eff,avg} = D_0 exp\left[\frac{-E_a}{RT}\right] \quad (6)$$

where T (K), E_a ($kJ.mol^{-1}$), R ($=8.3143 \times 10^{-3}$ $kJ.mol^{-1}.K^{-1}$), and D_0(m^2s^{-1}) are the absolute air temperature, activation energy, universal gas constant, and pre-exponential factor, respectively. E_a and D_0 could be assumed as constants in Eq. (6) provided that the temperature range is not large [44]. It is noted that in the Arrhenius equation, average moisture diffusivity $D_{eff,avg}$ ($m^2.s^{-1}$) is used, which can be defined as [45].

$$D_{eff,avg} = \frac{\int D_{eff}(M_{db}) dM_{db}}{\int dM_{db}} \quad (7)$$

For calculating$D_{eff,avg}$, Eq. (7) was solved numerically. In addition, Eq. (6) could be re-written in a linear form for E_a/R as below.

$$ln\left(D_{eff,avg}\right) = ln(D_0) - \left[\frac{E_a}{R}\right]\frac{1}{T} \quad (8)$$

There is a linear correlation between the values of $ln\left(D_{eff,avg}\right)$ and reciprocal of the absolute temperature 1/T. Thus, E_a/R could be evaluated by fitted slope using the plot of $ln\left(D_{eff,avg}\right)$ versus 1/T or directly via the coefficients of linear regression of $-ln\left(D_{eff,avg}\right) \sim 1/T$.

2.6. Color measurement

The color indicators of the product were monitored before and after drying in three replicates via a spectrophotocolorimeter (LabScan XE, Hunter Associates Laboratories, Inc., Reston, VA, USA) based on CIE L, a, and b color space. In Hunter scale, "L" represents the lightness with zero representing black and 100 referred to as white, "a" specifies redness with positive as a red, negative as a green and zero as gray, and finally "b" indicates yellowness with positive signifies yellow, negative as blue, and zero as gray. For each condition, three samples were taken and placed inside a 35-mm plastic dish (Corning, NY, USA) and the color variables were recorded. Then, the readings were used to find total color change (ΔE), darkness index (DI), visual observation index (VI), and Hue angle (H°) as follows [25,46]:

$$\Delta E = \sqrt{(\Delta L)^2 + (\Delta a)^2 + (\Delta b)^2} \quad (9)$$

$$DI = \frac{a}{b} \quad (10)$$

$$VI = \frac{L \times b}{a} \quad (11)$$

$$H^{\circ} = tan^{-1}\left(\frac{b}{a}\right) \quad (12)$$

where$\Delta L, \Delta a$, and Δb are$(L - L_{ref})$,$(a - a_{ref})$, and$(b - b_{ref})$, respectively and the reference parameters are considered the readings for the freeze-drying samples.

2.7. Microstructure of DDG by scanning electron microscope (SEM)

Micro-images of the surface of dried products were taken using an environmental scanning electron microscope (FEI Quanta FEG 450 ESEM, 231Hillsboro, OR, USA) operating at high vacuum mode (HV = 5 kV, Spot = 3.0, Pressure $\approx 6 \times 10^{-6}$ Torr). The samples were mounted on an SEM aluminum stub using a carbon adhesive tape before coating by gold/palladium with 7 nm thickness and micro-photographed at different magnifications.

2.8. Chemical composition analysis

Samples were sent to an external lab for wet chemistry analysis to find the chemical properties of the WDG and DDG, including crude protein, minerals, and fibers. For minerals, the samples were predigested

at ambient temperature for 10 min with 8 mL nitric acid (HNO3) and 2 mL hydrochloric acid (HCl) and then by an additional 10 min with 1 mL 30% hydrogen peroxide (H_2O_2). Then, they were digested via a CEM Microwave Accelerated Reaction System (MARS6) with a MarsXpress Temperature Control using 50 mL calibrated Xpress Teflon PFA vessels with Kevlar/fiberglass insulating sleeves before they were examined by ICP using a Thermo iCAP 6300 inductively coupled plasma radial spectrometer [47]. The acid detergent fiber (ADF) and neutral detergent fiber (NDF) were obtained according to ANKOM Technology Methods 14 and 15 and their solutions were made according to AOAC 973.18. ADF and NDF were tested two times for each samples to confirm the listed value. AOAC 990.03 has been used for protein content evaluation by measuring nitrogen by combustion. Here, 1 mm ground samples were analyzed by combustion using a CN628 Carbin/Nitrogen Determinator. ADF residue analyzed using a Leco TruMac N Macro Determinator to determine the protein fraction bound to the acid detergent fiber.

2.9. Statistical analysis of experimental data

The reported values are the mean values ± standard deviation, and at least four replications have been performed for each experiment. Statistical analysis was performed with R Ver. 4.0.3. General linear hypothesis (GLM) was used to perform multiple comparison procedures for ANOVA. The statistical significance of differences among the mean values was determined with Tukey's honestly significant difference test ($\alpha = 0.05$). Furthermore, all non-linear regression analyses for drying curve fittings were performed using Origin Lab 2019.

3. Results and discussion

3.1. Experimental drying curves and fitting of drying models

Statistics of experimental data fitted to six drying models (Table 1) were evaluated and detailed in Table 2. All the six models were able to yield a good fit to the drying data as shown by R^2 of near 1 and χ^2 of near zero (Table 2). The highest R^2 and the lowest χ^2 and *RSS* values can be seen in the Page and two-term models. In previous studies, with only two constants (k and n) to fit, the Page model and its modification were also selected as the best model for describing the drying kinetics of wheat grains [48], wheat distiller's grain with solubles dried using a conventional oven [49], microwave [50], and superheated steam [11]. The Page model parameter, *k*, can be used to compare the kinetics of drying between different conditions. The higher the *k* value, the higher the drying rate and the shorter the sample residence time [16]. The application of ultrasonic energy increased the value of *k* from 0.007, 0.0346, and 0.186 (min^{-1}) for HA at 25 °C, 50 °C, and 70 °C to 0.126, 0.316, and 0.346 (min^{-1}), an increase of 18-, 9-, and 2-folds, respectively (Table 2). This is an indication that drying time was decreased in the presence of ultrasonic waves, most significantly at 25 °C.

Drying curves, together with curve fitting to the Page model, and drying rates at three temperatures are illustrated in Fig. 2. Two different stages of drying can be observed on all the drying curves. The initial (short) period of drying is featured by a dramatic moisture removal where the drying rate reaches a maximum value. The fast drying at this stage should be originated from the highly accessible free surface moisture for removal. As the drying continues, the drying front diffuses inward and the bonded moisture inside the porous structure needs to

Table 2
Semi-empirical drying models and their statistical performance for all drying conditions.

Drying Conditions	Model	Constants	R^2	χ^2	RSS
HA 25 °C	Lewis Model	k = 0.02805	0.980	0.003	0.072
	Page Model	k = 0.00701, n = 1.36465	0.995	0.001	0.018
	Henderson and Pabis	a = 1.0515, k = 0.02934	0.983	0.002	0.061
	Logarithmic Model	a = 1.10889, k = 0.03299, b = −0.01385	0.972	0.009	0.222
	Two-term Model	a = −1011.05551, b = 1012.05289, k = 0.05278, m = 0.05274	0.995	0.001	0.019
	Midilli Model	a = 0.99742,b = −3.25694E-5, k = 0.00705, n = 1.36055	0.995	0.001	0.018
US 25 °C	Lewis Model	k = 0.06791	0.964	0.006	0.116
	Page Model	k = 0.12572, n = 0.81644	0.986	0.002	0.044
	Henderson and Pabis	a = 0.87189, k = 0.06172	0.972	0.005	0.091
	Logarithmic Model	a = 0.88433, k = 0.06321, b = 0.00154	0.974	0.005	0.085
	Two-term Model	a = 0.52179, b = 0.47644, k = 0.12566, m = 0.04649	0.987	0.003	0.043
	Midilli Model	a = 1.00736, b = −9.95838E-6, k = 0.13546, n = 0.79404	0.987	0.002	0.042
HA 50 °C	Lewis Model	k = 0.05812	0.995	0.000	0.010
	Page Model	k = 0.03465, n = 1.1605	0.997	0.000	0.006
	Henderson and Pabis	a = 1.00803, k = 0.05845	0.995	0.001	0.010
	Logarithmic Model	a = 1.01244, k = 0.05746, b = −0.0053	0.995	0.001	0.009
	Two-term Model	a = −0.26421, b = 1.26421, k = 2.39347, m = 0.06864	0.997	0.000	0.006
	Midilli Model	a = 1.00054, b = 5.74636E-5, k = 0.03307, n = 1.17782	0.997	0.000	0.006
US 50 °C	Lewis Model	k = 0.16475	0.981	0.004	0.068
	Page Model	k = 0.31594, n = 0.75642	0.995	0.001	0.019
	Henderson and Pabis	a = 0.98138, k = 0.16304	0.982	0.004	0.067
	Logarithmic Model	a = 0.98297, k = 0.16545, b = 0.00134	0.984	0.004	0.057
	Two-term Model	a = 0.72462, b = 0.27553, k = 0.25033, m = 0.09504	0.995	0.001	0.018
	Midilli Model	a = 1.00054, b = 5.74636E-5, k = 0.03307, n = 1.17782	0.995	0.001	0.018
HA 70 °C	Lewis Model	k = 0.14922	0.987	0.003	0.034
	Page Model	k = 0.18543, n = 0.0612	0.988	0.003	0.031
	Henderson and Pabis	a = 0.99545, k = 0.1489	0.987	0.003	0.034
	Logarithmic Model	a = 0.99676, k = 0.14998, b = 4.5331E-4	0.988	0.003	0.032
	Two-term Model	a = 0.88384, b = 0.11928, k = 0.16756, m = 0.08989	0.986	0.003	0.028
	Midilli Model	a = 1.00203, b = 2.67138E-6, k = 0.1814, n = 0.93079	0.988	0.003	0.030
US 70 °C	Lewis	k = 0.18992	0.982	0.003	0.063
	Page model	k = 0.345, n = 0.05857	0.986	0.003	0.050
	Henderson and Pabis	a = 0.99383, k = 0.18944	0.982	0.003	0.063
	Logarithmic model	a = 0.99448, k = 0.19064, b = 4.38236E-4	0.983	0.003	0.059
	Two term	a = 0.81953, b = 0.18147, k = 0.23397, m = 0.11291	0.987	0.003	0.047
	Midilli	a = 1.0008, b = −3.73639E-7, k = 0.29393, n = 0.83247	0.986	0.003	0.050

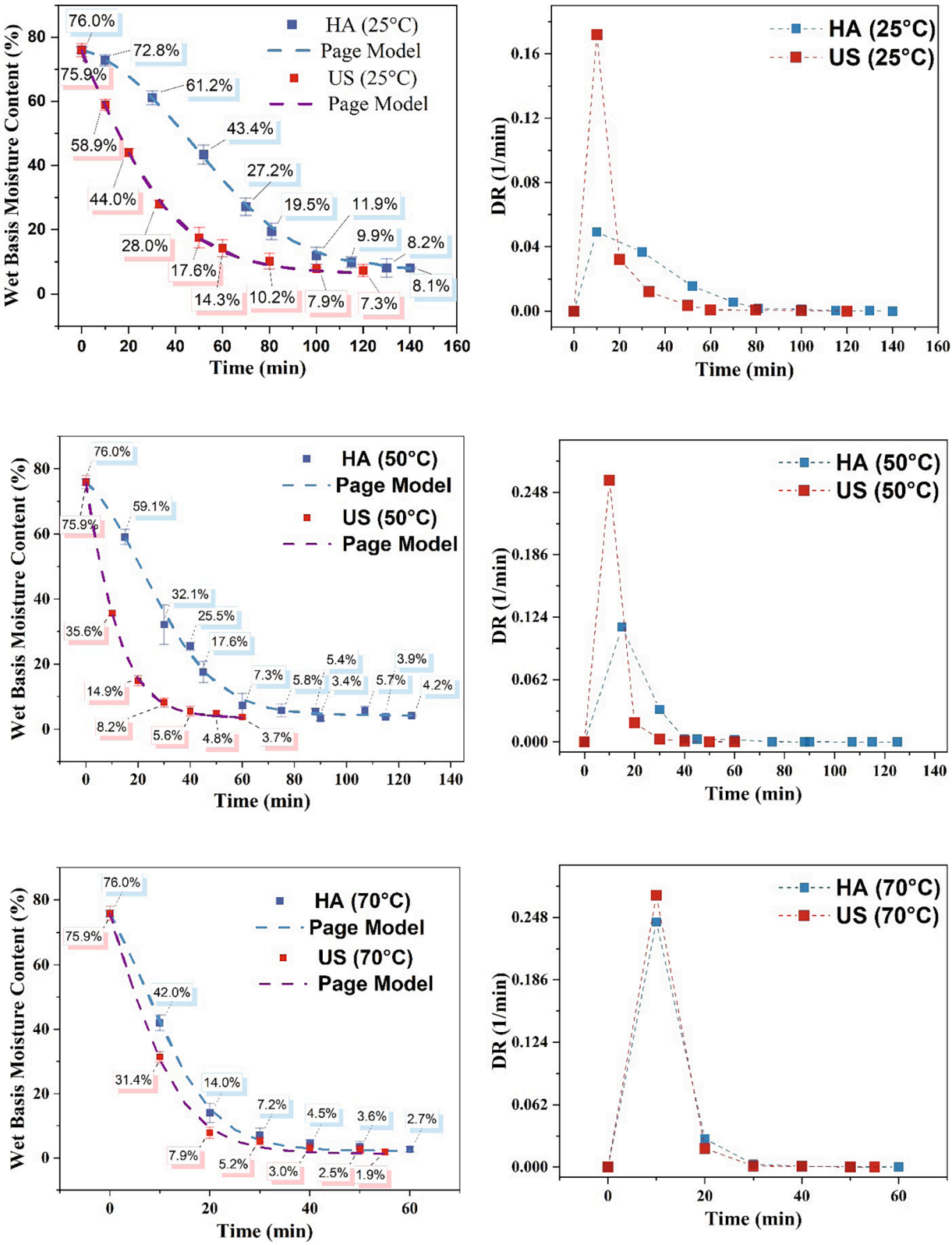

Fig. 2. Comparing the drying curves and drying rate of DDG at different temperatures with and without using ultrasound power.

migrate to the surface to be removed. Thus, the drying rate decreases till it reaches equilibrium moisture content $M_{wb,eg}$. In addition, the vapor pressure gradient between the sample and surrounding air, being the driving force behind moisture migration, decreases as the moisture content decrease, resulting in a decreasing drying rate. Increasing the drying temperature from 25 °C to 70 °C enhanced the drying rate and reduced the drying time (Fig. 2) as the heat and mass transfer coefficients went up with the temperature, leading to a higher moisture gradient. These phenomena were also reported in other studies dealing with thin-layer drying [49,51].

The application of ultrasound reduced the drying time and increased the drying rate in all experiments, especially at the initial stages of

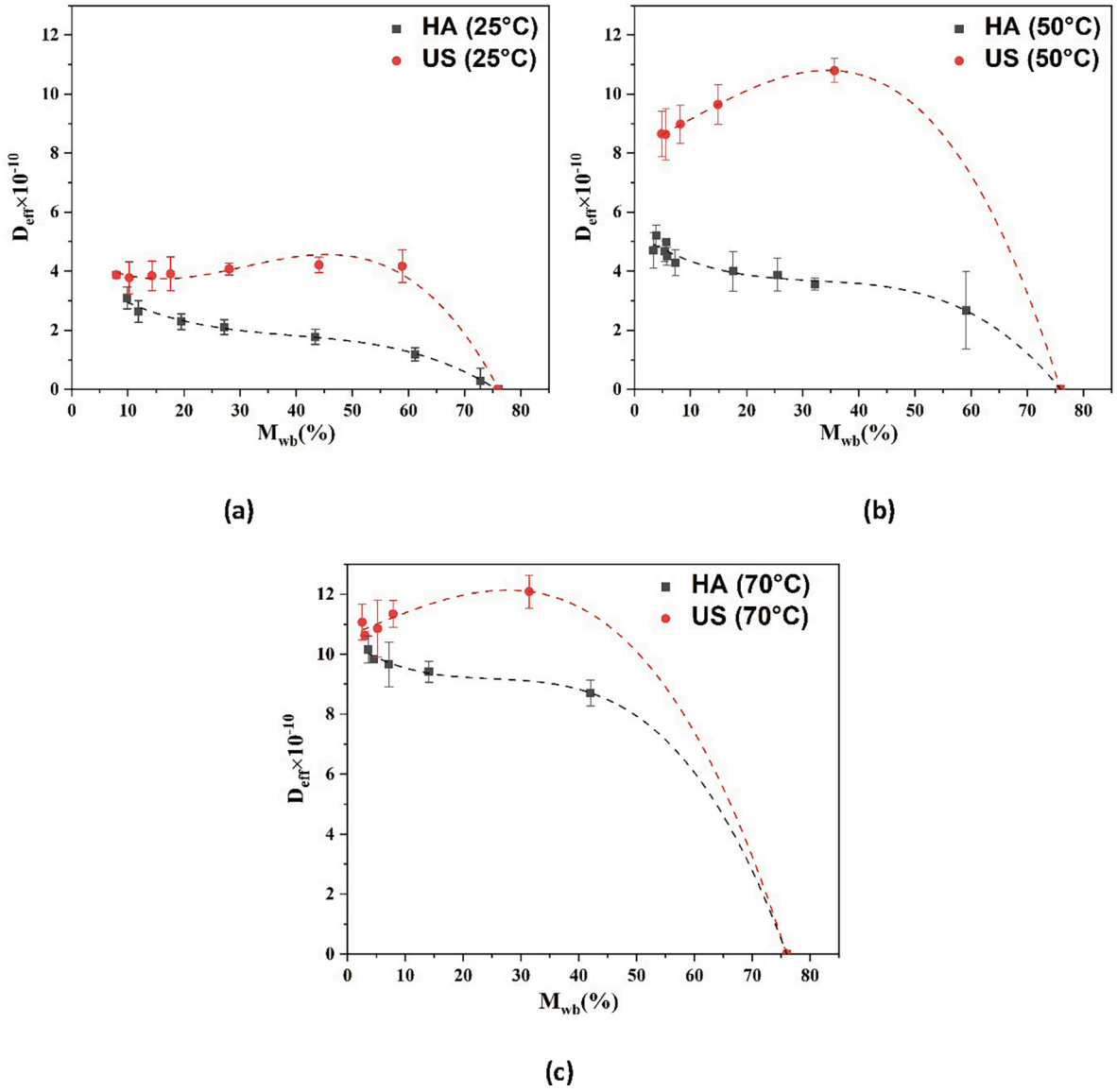

Fig. 3. Comparing the effective moisture diffusivity versus wet basis moisture content for HA drying and US drying at (a) 25 °C, (b) 50 °C, and (c) 70 °C.

drying (Fig. 2). A unique feature of this direct-contact ultrasonic dehydration system is that the drying surface undergoes vibration at ultrasonic frequency modulated by MMM technology which may facilitate vibrational moisture removal in the form of misting when moisture content is high. In essence, the relative magnitude of the surface tension at the liquid–air interface and ultrasonic vibrational force controls the droplet formation [24]. This obviates the necessity in ultrasonic drying to warm-up and the free moisture on the product surface turns into mist instantly when ultrasonic vibration is introduced, thereby most of the surface water could be removed rapidly [52]. In addition, it would be interesting to delineate the effect of moistest removal mediated by vibration and that by acoustic cavitation. Fig. 2 illustrates that the improvement in drying rate due to ultrasound is more significant at the initial stages of the drying, particularly at lower temperatures. The underlying reason for enhanced drying rate at the initial stage of drying might be the quick removal of free surface moisture by ultrasound, with no warm-up period. Furthermore, the improvement of drying rate by ultrasound becomes less significant at a higher temperature. For drying at 25 °C, for instance, the application of ultrasound increased the initial drying rate by nearly 3.5 times, from 0.049 min^{-1} (without ultrasound) to 0.17 min^{-1} (with ultrasound) while for drying at 70 °C, the drying rate was increased by only approximately 10%, from 0.244 min^{-1} (without ultrasound) to 0.27 min^{-1} (with ultrasound). Another finding in ultrasonic drying is that a lower equilibrium moisture content $M_{wb,eg}$ can be achieved in ultrasonic drying at all temperatures. $M_{wb,eg}$ for HA was found to be 8.1%, 4.2%, and 2.7% at temperatures of 25 °C, 50 °C, and 70 °C respectively. Similar results were reported by Mosqueda and Tabil [50] for forced convection hot air drying of wheat DDG where $M_{wb,eq}$ was found to be 4.62%, 3.17%, and 2.15% at temperatures of 40 °C, 60 °C, and 80 °C, respectively. In this study, ultrasonic drying decreased the equilibrium moisture content ($M_{wb,eg}$) from 8.1% to 7.3%, 4.2% to 3.7%, and 2.7% to 1.9% compared to HA at 25 °C, 50 °C, and 70 °C, respectively. Reducing $M_{wb,eq}$ is expected to decrease the caking up process in DDG transportation and increase the shelf life of the product [53]. *Mwb,eg* for thermal drying process depends on relative humidity, temperature, and the bonding of water molecules with biopolymeric materials. The presence of ultrasonic waves and the high frequency vibration might have loosened the bonding of water molecules with proteins, fibers, and other components in the DDG, as evidenced by a lower activation energy, thus more water molecules can escape from the structure during drying, resulting in a lower $M_{wb,eg}$. In addition, mechanical removal of water due to ultrasound does not

depend on the thermodynamic equilibrium between the vapor pressure of the air and the water in the product structure. Thus, ultrasonic drying could result in a dried product with less moisture content.

3.2. Evaluation of moisture diffusivity

Effective moisture diffusivity is a key indicator of drying hydrodynamic and is commonly used to identify mostly the mass transfer mechanisms in a drying process. Since drying of DDG occurred mostly in the falling rate period, diffusion was considered as the main mechanism of dehydration, and thus Eq. (4) was used to obtain the effective moisture diffusivity (D_{eff}). Fig. 3a-3c show the variation of D_{eff} versus wet basis moisture content for HA and US at different temperatures. The D_{eff} varied considerably with M_{wb} and its trend is different for HA and US. For HA drying, decreasing M_{wb} led to an increase in D_{eff} and it continued decreasing exponentially with decreasing M_{wb} until it reached the equilibrium moisture content. For US drying, however, D_{eff} increased sharply in the initial stage of the drying and then decreased gradually with reducing M_{wb}. This may be attributed to the fact that D_{eff} is comprised of both vapor/mist and liquid diffusivities [54–55]and the diffusivity of moisture in the gas/vapor phase is higher than that in liquid form [56].

For HA drying, in the initial stage of drying where water exists in great amounts, liquid diffusion is dominant while in the later stage of drying, the moisture content decreases, and moisture removal principally happens as a result of vapor diffusion, thus having a high effective diffusivity. More discussion on the effects of temperature on effective diffusivity can be found in the work of Çağlar et al. [58] and Pathare and Sharma [57]. However, in the US, the ultrasonic wave's impact on the liquid molecules was higher than the vapor. There exists a large impedance mismatch between the vibrating metal sheet transmitting ultrasonic waves and vapor in the pore structures of the sample, compared to that for water. Thus, moisture in the liquid phase absorbs ultrasonic waves more efficiently than in the gas phase. Consequently, due to enhanced liquid diffusivity, the D_{eff} in the presence of ultrasonic waves had a greater value, especially at low temperatures. For example, at 25 °C, US enhanced D_{eff} by around 2.5 times from 1.19×10^{-10} to 4.17×10^{-10} m^2s^{-1} at $M_{wb} = 60\%$. Interestingly, the effect of US at high temperature (70 °C) and low moisture content ($M_{wb} < 10\%$) is diminished such that the D_{eff} only increased from just over 10×10^{-10} to 11×10^{-10} m^2s^{-1}, an increase of around 9%. In sum, the impact of US on effective diffusivity was more evident at low temperature and high moisture content. Also, the D_{eff} in this study was in the same range as the one pertained to distiller's spent grain (3.24×10^{-10} to 2.4×10^{-9} m^2s^{-1}) as reported by Zielinska et al. [51].

Table 3 shows the average effective moisture diffusivity ($D_{eff,avg}$) obtained using Arrhenius equation (Eq. (7)) and drying time for each drying method at temperatures of 20 °C, 50 °C, and 70 °C. $D_{eff,avg}$ and drying time are two important drying parameters for comparing the impact of US on drying kinetics at different temperatures. For HA, increasing temperature from 25 °C to 70 °C increased $D_{eff,avg}$ from 1.03 $\times 10^{-10}$ to 8.99 $\times 10^{-10}$ while it decreased the drying time from 140 min to around 26 min. For US drying, the same increment in temperature enhanced $D_{eff,avg}$ from 4.11×10^{-10} to 11.8×10^{-10} and decreased drying time from 84 min to 20 min. The increasing $D_{eff,avg}$ with temperature should be attributed to augmented heat and mass transfer between the heating media and solid matrix. Compared to hot-air drying and to reach a final moisture content of 8 to 9 % (wet basis), ultrasonic drying in combination with air at different temperatures reduced drying time by 40%, 46%, and 23% for air temperatures of 25 °C, 50 °C, and 70 °C, respectively. US + HA at 50 °C seems to be the optimal condition for drying of DDG that can achieve maximized drying enhancement by the application of ultrasound.

Table 3
Comparison of effective diffusivity and drying time for hot air drying (HA) and ultrasonic drying (US) at different temperature.

Temperature (∘C)	Average effective diffusivity ($\times 10^{-10}$ m^2/s)		Average effective diffusivity enhancement by US (%)	Drying time (min)	
	HA Drying	US Drying		HA Drying	US Drying
25	1.03 (±0.18)	4.11 (±0.21)	298	140	84
50	3.31 (±0.45)	10.15 (±0.23)	207	60	32
70	8.99 (±0.22)	11.78 (±0.26)	31	26	20

3.3. Activation energy

Activation energy (E_a), or activation energy barrier, indicates how much energy is required to activate and remove one mole of water molecules from a solid matrix during a drying process and therefore depends on moisture-matrix bonding. The energy of drying increases as the E_a goes up. The E_a of DDG was calculated based on Eq. (8) and the fitting results are shown in Fig. 4. E_a can be determined from the slope in the chart (E_a/R) for each drying method. The E_a for US and HA was 20.5 kJ/mol and 40.6 kJ/mol, respectively. Thus, drying DDG in the absence of ultrasonic vibrations would be twice more difficult (energy-consuming). The E_a for HA is close to that for distillers' spent grain fraction (DSG) from stillage dried with superheated steam (53.74 kJ/mol), as reported by Zielinska et al. [51].

The obtained E_a values for HA and US could be used to analyze possible moisture removal mechanisms in each drying method. It can be seen that the energy required to initiate HA drying of DDG, e.g. an E_a of 40.6 kJ/mol, is close to the heat of vaporization of water (45 kJ/mol). Thus, evaporation is a dominant mode for moisture removal in HA of DDG. On the other hand, an E_a of 20.5 kJ/mol for US drying of DDG may indicate that vaporization is not dominant in this drying process. The energy consumption in US drying should be associated with other mechanisms for moisture removal, such as misting induced by ultrasonic vibration where no phase change is involved in water removal. In addition, the vibration may loosen the binding between water molecules and the product matrix. As a result, the moisture removal from DDG in the US process can take place at a much lower energy level. Baini and Langrish [60] and Debenedetti [59] reported that 20 kJ/mol is the amount of energy that corresponded to hydrogen bond strength.

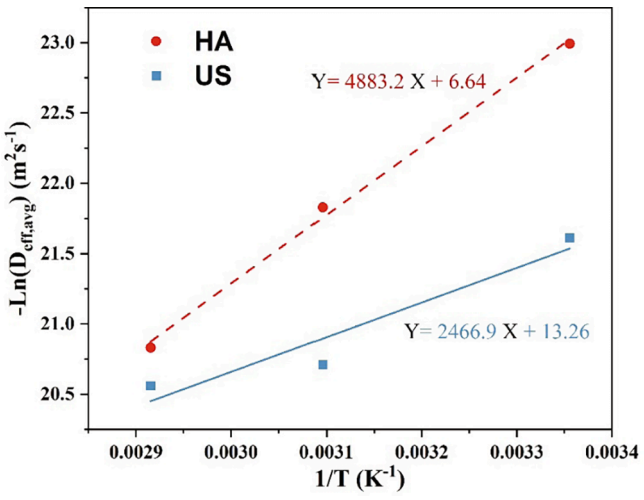

Fig. 4. Effective diffusivity versus wet basis moisture content for HA drying (a) and US drying (b) at different temperatures ($Y = -ln(D_{eff,avg})$, $X = 1/T$).

Table 4
Color readings of WDG and different treatments of DDG.

Color parameters	WDG	DDG (FD)	DDG (US 25 °C)	DDG (HA 50 °C)	DDG (HA 70 °C)
L	79.4 (0.378) [a]	96.1 (0.473) [a]	80.2 (1.12) [a]	75.4 (0.389) [b]	75.7 (0.118) [b]
a	6.44 (0.077) [a]	3.68 (0.11) [b]	7.32 (0.405) [b]	7.75 (0.297) [c]	8.54 (0.202) [d]
b	39.9 (0.202) [a]	31 (0.439) [b]	35.7 (1.47) [b]	33.5 (1.31) [c]	35.7 (0.425) [b]

[a-d] Same superscript letter for each color parameter indicates no significant difference among treatments ($p > 0.05$).

3.4. Color change

Color of DDG has traditionally been used as an indicator of heat damage and amino-acid digestibility and played an important role in quality assessment in the community [61–62]. Furthermore, as currently there is no grading system to differentiate the quality of DDG, color has been used as a subjective indicator for quality evaluation and pricing. In essence, a price differentiation of 20 $ to 30 $/ton market price exists between darker and lighter DDG [18]. Here, the color values of WDG and the DDG dried with/under 4 drying methods/conditions are tabulated in Table 4. The treatments were freeze drying (FD), direct-contact ultrasonic drying at 25 °C (US25), hot air drying at 50 °C (HA50), and hot air drying at 70 °C (HA70) with WDG as the control. Freeze drying was used as the reference for calculating the total color change and comparing different dried products. Table 4 shows that the color indicators in the US-dried DDG are closer in value to the freeze-dried in terms of lightness (*L*) and yellowness (*b*). As the temperature increases, the redness indicator of the material increases (the value of "*a*" was 7.32 and 8.54 for US25 and HA70, respectively), and the color of the final product becomes darker ("*L*" decreases from 80.2 (US25) to

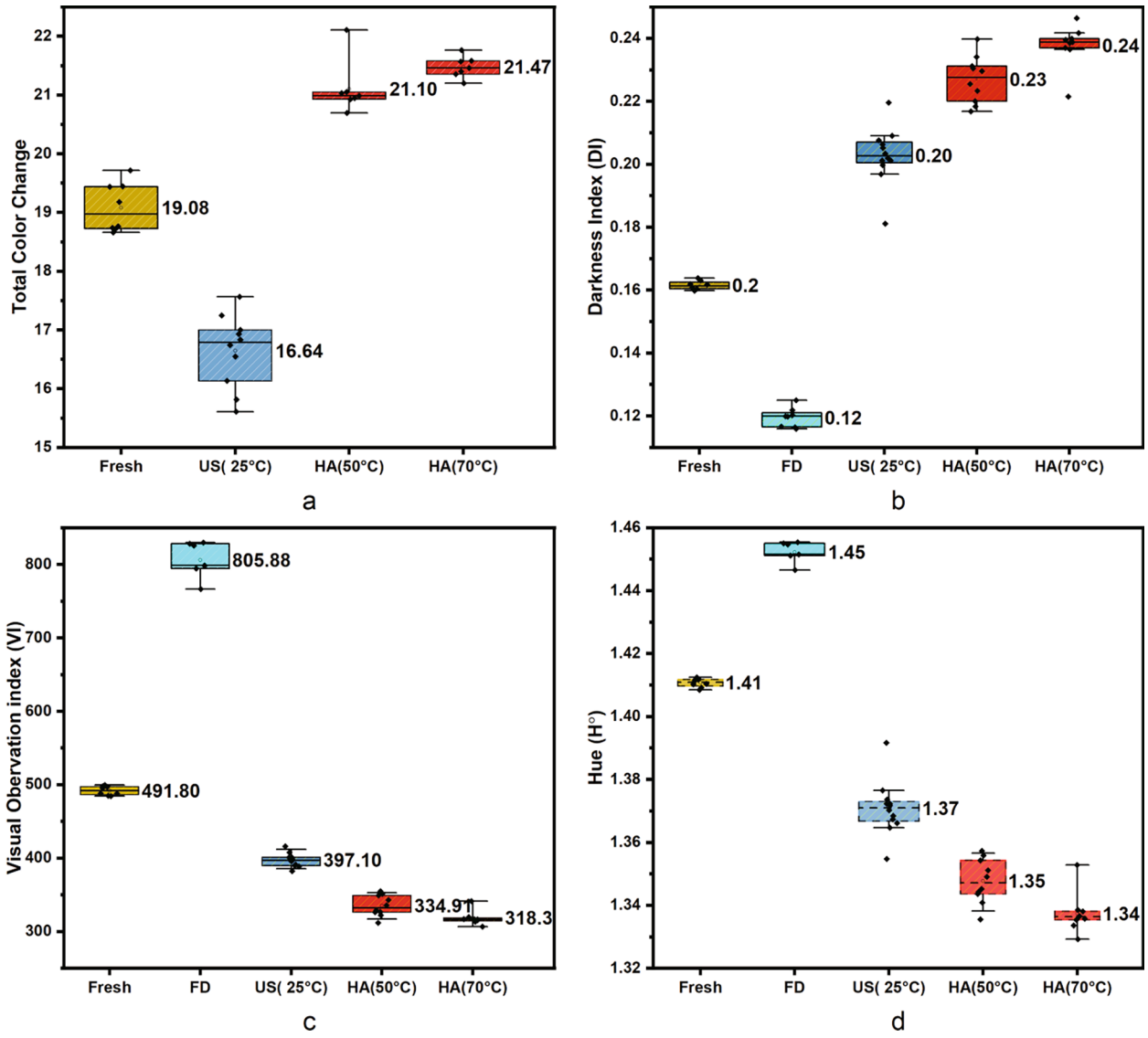

Fig. 5. Total color change (a), Darkness index (b), Visual observation index (c), and Hue angle (d) for DDG products dried with different methods.

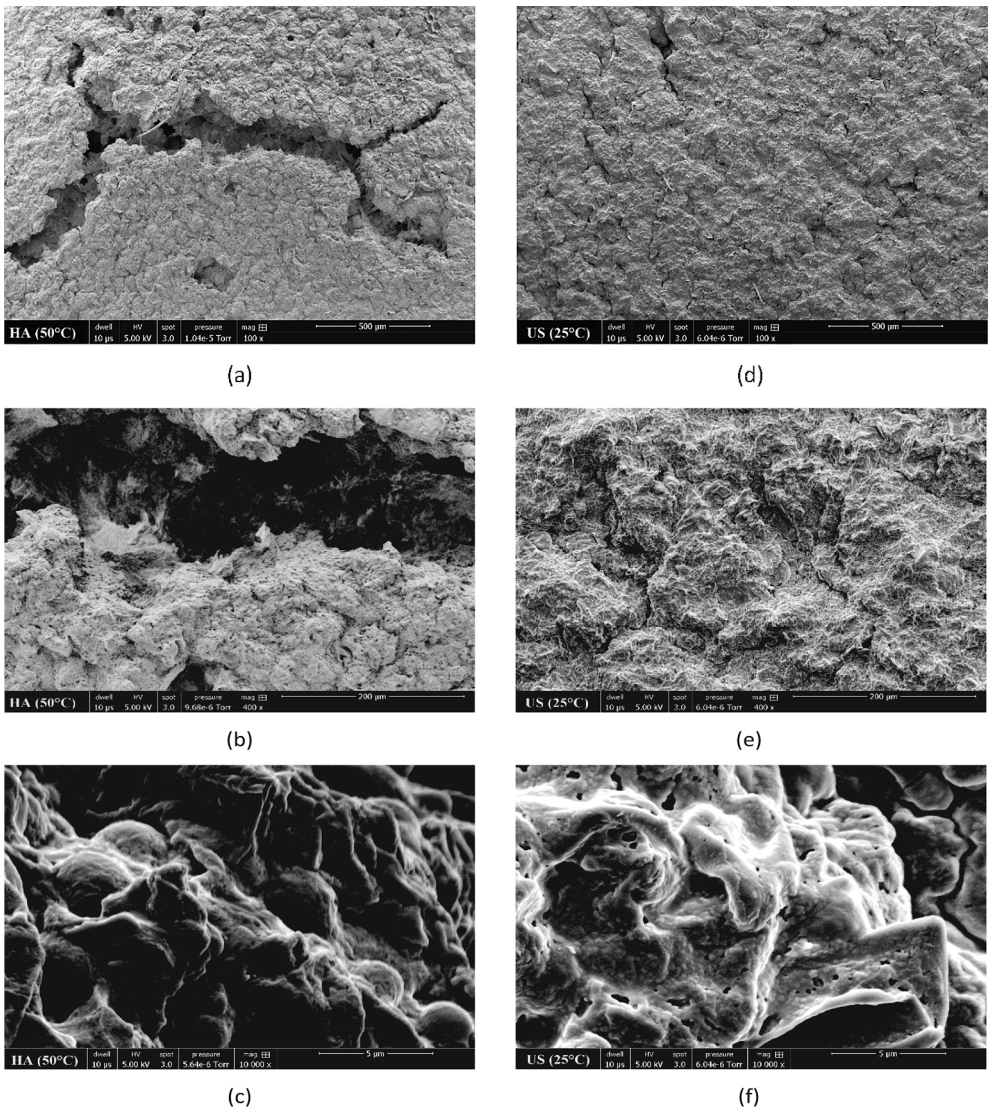

Fig. 6. ESEM micro-images of DDG dried with hot air at 50 °C (a,b,c) and ultrasound (d,e,f) at different magnifications.

75.7 (HA70)). The decreasing of "*L*" of DDGS with increasing temperature was in agreement with the report of Mosqueda and Tabil [50]. Sample darkening is a result of material exposure to elevated temperatures during drying and is attributed to the Maillard reaction. It is well-documented that a rise in temperature and exposure time accelerates the rate of Maillard reaction and color development [63–64]. Ultrasonic non-thermal drying is not in favor of the Maillard reaction and reduced color change can be attributed to shorter drying time (less exposure) and the low temperatures in the process. In contrary, samples in HA drying are exposed to relatively high temperatures for a longer period, drying up the surface of the food gradually, forming a crust with low water activity at the surface, and promoting the Maillard reaction rate [65]. Drying in the absence of hot air at a shorter time, such as in US drying, decreases the Maillard reaction and leads to a product with a much lighter color.

Table 5
Chemical properties of distiller's grain.

Components	WDG	DDG (FD)	DDG (US 25 °C)	DDG (HA 50 °C)	DDG (HA 70 °C)
Crude Protein (%)	52.45 (0.35) ^{b}	53.83 (0.1528) ^{a}	52.47 (0.5737) ^{b}	52.2 (0.22) ^{b}	52.3 (0.26) ^{b}
Available Protein (%)	46.65 (0.07) ^{a}	42.4 (0.72) ^{b}	46.37 (1.63) ^{a}	43.7 (0.33) ^{b}	42.6 (0.46) ^{b}
Adjusted Crude Protein (%)	47.65 (0.07) ^{a}	43.43 (0.72) ^{b}	47.37 (1.63) ^{a}	44.7 (0.33) ^{ab}	43.6 (0.46) ^{b}
ADICP (%)	5.85 (0.35) ^{c}	11.43 (0.777) ^{a}	6.08 (1.19) ^{c}	8.50 (0.41) ^{b}	9.73 (0.723) ^{ab}
ADF (%)	16.35 (1.48)	17.3 (2)	14.42 (1)	14. 7 (1.6)	14.93 (1.2)
NDF (%)	30.15 (1.34)	30.83 (5)	30.82 (3)	33.27 (3)	31.67 (2.9)
TDN (%)	82.5 (0.71)	80.33 (1.53)	82.5 (1.3)	80.7 (0.96)	80.67 (0.58)

The results are in dry matter (DM).
No Tukey letters refers to insignificant differences among all the values.
Values in parenthesis represents the standard deviation.
$^{a\text{-}d}$ Same superscript (tuckey) letter for each component indicates no significant difference among treatments ($p > 0.05$).

Table 6
Mineral contents of distiller's grain.

Components	WDG	DDG (FD)	DDG (US 25 °C)	DDG (HA 50 °C)	DDG (HA 70 °C)
Calcium (%)	0.02 (0)	0.02 (0)	0.02 (0)	0.02 (0)	0.02 (0)
Phosphorus (%)	0.6 (0.14)	0.64 (0.02)	0.62 (0.020)	0.62 (0.017)	0.65 (0.025)
Magnesium (%)	0.13 (0.03)	0.13 (0.012)	0.135 (0.006)	0.13 (0.0082)	0.14 (0.01)
Potassium (%)	0.47 (0.099)	0.43 (0.055)	0.4225 (0.034	0.4175 (0.035)	0.46 (0.026)
Sodium (%)	0.013 (0)	0.0097 (0.0025)	0.00875 (0.0017)	0.008 (0.0022)	0.0077 (0.0015)
Iron (ppm)	115 (1.4) [a]	86 (0) [b]	90.25 (3.3) [b]	90.25 (5.1) [b]	88.67 (2.31) [b]
Zinc (ppm)	62 (14.14)	62.33 (2.90)	62.5 (1.30)	63.25 (2.22)	66.33 (0.58)
Copper (ppm)	7.5 (2.12)	6.67 (0.58)	7.25 (1.90)	7.25 (1.50)	7 (0)
Manganese (ppm)	9.5 (0.71)	7.67 (0.58)	8.5 (1)	7.75 (0.50)	8.33 (0.58)

The results are in dry matter (DM).
Values in parenthesis represent the standard deviation.
[a-b] Same superscript letter for each component indicates no significant difference among treatments ($p > 0.05$). No Tukey letters refers to insignificant differences among all the values.

4. Values in parenthesis represents the standard deviation.

The yellow color development (index "*b*") seems to depend on both drying temperature and time as it decreases with a rise in temperature and a drop in the drying time. Total color change (ΔE), darkness index (*DI*), visual observation index (VI), and Hue angle (H°) are shown in Fig. 5a-d, respectively. Mean values of the data are placed next to each box plot. Generally, a greater color change can be observed with increasing temperature. There was a significant difference between the color indicators of the ultrasonic (25 °C) and HA-dried samples, but the difference between the HA samples at 50 °C and 70 °C was statistically insignificant. In fact, an increase in temperature from 25 °C to 50 °C was more detrimental to the color of DDG than increasing it from 50 °C to 70 °C. From Fig. 5a, it can be seen that the least total color change from the freeze-dried sample belongs to the ultrasonic drying ($\Delta E \approx 16.64$) and it increases significantly for HA drying method at T = 50 °C to around 21.10 and the rising trend continues slowly to around 21.47 for the samples dried at 70 °C by HA. Fig. 5b, 5c, and 5d show that the darkness index, visual observation index, and hue angle of the ultrasonic dried product were closer to the fresh product (WDG).

4.1. Surface structure of DDG by scanning electron microscope (SEM)

Micro-images of the HA- and US-dried DDG were taken using scanning electron microscopy and are shown in Fig. 6. Fig. 6a-c represent the HA-dried DDG while Fig. 6d-f signify the US sample at different magnifications. Comparing Fig. 6a-b with 6d-e, it can be seen that relatively large cracks are formed on HA-dried DDG surface while the US-dried one remains relatively smooth with smaller cracks and pores over the entire surface. Looking closely at the higher magnification in Fig. 6c and 6f, it can be seen that ultrasound produces numerous fine pores on the sample surface which provide channels allowing internal moisture to come to the sample surface during drying. This could be part of the reason why ultrasonic drying has achieved a significantly higher drying rate and shorter drying time compared to HA. The fine holes on the surface as a result of the mechanical action of ultrasound are in line with the observations reported by Gu et al. [66] on DDG residue. The exact reason for the formation of tiny holes on DDG surface is not known. It will be an interesting topic for future study.

4.2. Chemical composition analysis and minerals

Although a light-colored sample often indicates a better quality of DDG, wet chemistry for evaluating the chemical compositions of DDG still is the most acceptable method for assessing the quality of DDG. Table 5 compares the percentage of crude protein, available protein, adjusted crude protein, ADICP (acid detergent insoluble crude protein), adjusted crude protein, ADF (acid detergent fiber), NDF (neutral detergent fiber), and TDN (total digestible nutrients) for WDG as well as DDG dried with different techniques (FD, US25, HA50, and HA70). It can be observed that the percentage of crude protein is not significantly affected by drying method and temperature with 52.47%, 52.2%, and 52.3% for US25, HA50, and HA70, respectively. Available protein, however, decreases for all dried products except US25. No statistical difference between WDG and US25 indicates that US treatment does not affect the available protein of the final product in contrast to other drying processes. Freeze-dried DDG also has a significantly lower available protein than the US sample. The relatively high temperature (45 °C) in the secondary drying stage and long drying time for FD might be the underlying cause of the reduction in available protein. ADICP is a useful indicator of protein quality and represents the indigestible fraction of protein related to heat damage. It is the recovered crude protein from acid detergent fibers. The higher the value of ADICP, the greater the heat damage [67]. As it can be seen, US25 gives the lowest ADICP of 6.08% with no significant statistical difference with the fresh product (5.85%), indicating negligible damage to digestible protein. Increasing the temperature deteriorated the protein quality and increased ADICP to 8.50% at 50 °C and 9.73% at 70 °C, exacerbating the percentage of the heat-damage protein by around 40% and 60%, respectively. The results have consistency with hot air dried wheat DDG obtained by Mosqueda et al. [16] in both the ADICP values and their trend with air temperature, which was in the range of 8.95–10.67% for the temperature of 40–120 °C. Greater values of ADICP were believed to be a result of high temperatures, which produces more insoluble and intensifies the Maillard reaction. Furthermore, the slow drying process in FD leads to the worst proportion of ADICP of 11.43%, corroborating the fact that both the drying temperature and time are influential on the final quality of DDG. No statistically significant differences were observed for ADF, NDF, and TDN among all the drying processes.

Tracking the levels of minerals is consequential for a DDG production unit. For example, overabundant phosphorus and sodium in the feed pose risks to the environment or livestock. High levels of sodium can increase water consumption and wet litter, thereby leading to additional bacterial growth and infections. Phosphorus represents the most potential risk to the environment and hence its level in the diet should be well-controlled for optimum animal performance with minimum environmental impact. The suitable range of phosphorus in DDG can be between 0.62% and 0.77% while for the sodium it ranges from 0.05% to 0.17% [68]. Comparing minerals such as calcium, phosphorus, magnesium, potassium, sodium, iron, zinc, copper, and manganese in Table 6 illustrates that all the dried products, irrespective of the drying time, temperature, and the mechanisms of water removal, would possess the same levels of minerals. These data will cast off the idea of producing dissolved minerals by mist production in ultrasonic drying. This is an important issue in using ultrasonic dewatering techniques [69]as they may disperse minerals to the air and might cause environmental risks. Thus, the moisture removed from DDG by the US will not carry out any minerals and would be similar to the evaporation process in traditional

dryers.

5. Conclusion

The MMM ultrasonic drying significantly enhanced the drying process as shown by increased drying rate and effective moisture diffusivity, and reduced drying time. Under non-thermal condition (25 °C), a 3.5-time increase in drying rate in the initial stage of drying, a 300% augment in average effective moisture diffusivity, and a reduction of drying time from 140 min to 84 min was achieved in US drying. The DDG dried using US at 25 °C was featured by a brighter color, higher available protein, and smoother surface. No significant difference in acid detergent insoluble crude protein between the ultrasound-dried DDG at 25 °C and fresh product indicated that there was no/less heat damage during ultrasonic drying. The required activation energy of dehydration of DDG using the developed direct-contact ultrasonic dryer was found to be about half of the conventional hot air dryer. In sum, the best performance of ultrasonic waves in enhancing the drying kinetics and nutrient profile of DDG at low temperature opens a door towards developing sustainable, rapid, and non-thermal dehydration technology for DDG production.

Declaration of Competing Interest

The authors declare that they have no known competing financial interests or personal relationships that could have appeared to influence the work reported in this paper.

Acknowledgment

This work was supported by the United States Department of Energy under grant no. DOE-DE-EE0009125, USDA NIFE award # 2018-67017-27913, and NSF award #NSF IIP 16-24812 I/UCRC IA.

References

[1] D. of Department of Energy, Ethanol Production and Distribution, (2020). https://afdc.energy.gov/fuels/ethanol_production.html.
[2] K. Davis, Corn milling, processing and generation of co-products, in: 62nd Minnesota Nutr. Conf. Minnesota Corn Grow. Assoc. Tech. Symp., Bloom. MN, 2001.
[3] X. Wang, Y. Wang, B. Wang, H. Blaschek, H. Feng, Z. Li, Biobutanol production from fiber-enhanced DDGS pretreated with electrolyzed water, Renew. Energy. 52 (2013) 16–22, https://doi.org/10.1016/j.renene.2012.10.011.
[4] T. Klopfenstein, Distillers grains as an energy source and effect of drying on protein availability, Anim. Feed Sci. Technol. 60 (3-4) (1996) 201–207.
[5] U.S. Grains Council, Distiller ' s dried grains with solubles (DDGS), U.S. Grains Counc. (2012).
[6] G.C. Shurson, Issues and opportunities related to the production and marketing of ethanol by-products, 2005. https://doi.org/10.22004/ag.econ.32880.
[7] M.J. Spiehs, M.H. Whitney, G.C. Shurson, Nutrient database for distiller's dried grains with solubles produced from new ethanol plants in Minnesota and South Dakota, J. Anim. Sci. 80 (2002) 2639–2645.
[8] R.L. Belyea, K.D. Rausch, M.E. Tumbleson, Composition of corn and distillers dried grains with solubles from dry grind ethanol processing, Bioresour. Technol. 94 (2004) 293–298, https://doi.org/10.1016/j.biortech.2004.01.001.
[9] C. Clementson, K.E. Ileleji, R.L. Stroshine, Particle segregation within a pile of bulk Distillers Dried Grains with Solubles (DDGS) and variability of nutrient content, Cereal Chem. 86 (3) (2009) 267–273.
[10] H.H. Stein, M.L. Gibson, C. Pedersen, M.G. Boersma, Amino acid and energy digestibility in ten samples of distillers dried grain with solubles fed to growing pigs, J. Anim. Sci. 84 (2006) 853–860.
[11] Z. Tang, S. Cenkowski, M. Izydorczyk, Thin-layer drying of spent grains in superheated steam, J. Food Eng. 67 (2005) 457–465, https://doi.org/10.1016/j.jfoodeng.2004.04.040.
[12] S. Świątkiewicz, J. Koreleski, The use of distillers dried grains with solubles (DDGS) in poultry nutrition, Worlds. Poult. Sci. J. 64 (2008) 257–266, https://doi.org/10.1017/S0043933908000044.
[13] A.R.P. Kingsly, K.E. Ileleji, C.L. Clementson, A. Garcia, D.E. Maier, R.L. Stroshine, S. Radcliff, The effect of process variables during drying on the physical and chemical characteristics of corn dried distillers grains with solubles (DDGS)–Plant scale experiments, Bioresour. Technol. 101 (1) (2010) 193–199.
[14] C.L. Clementson, K.E. Ileleji, Particle heterogeneity of corn distillers dried grains with solubles (DDGS), Bioresour. Technol. 107 (2012) 213–221.
[15] R. Bhadra, K. Muthukumarappan, K.A. Rosentrater, Effects of CDS and drying temperature levels on the flowability behavior of DDGS, Dry. Technol. 30 (5) (2012) 542–558.
[16] M.R.P. Mosqueda, L.G. Tabil, C. Christensen, Effect of drying conditions and level of condensed distillers solubles on protein quality of wheat distillers dried grain with solubles, Dry. Technol. 31 (2013) 811–824, https://doi.org/10.1080/07373937.2013.765446.
[17] R.L. Belyea, K.D. Rausch, T.E. Clevenger, V. Singh, D.B. Johnston, M.E. Tumbleson, Sources of variation in composition of DDGS, Anim. Feed Sci. Technol. 159 (2010) 122–130, https://doi.org/10.1016/j.anifeedsci.2010.06.005.
[18] J. Shurson, S. Noll, Feed and alternative uses for DDGS, St. Louis, 2005. https://doi.org/10.22004/ag.econ.7623.
[19] J.D. Murphy, N. Power, How can we improve the energy balance of ethanol production from wheat? Fuel. 87 (2008) 1799–1806, https://doi.org/10.1016/j.fuel.2007.12.011.
[20] Y. Zhang, N. Abatzoglou, Review: Fundamentals, applications and potentials of ultrasound-assisted drying, Chem. Eng. Res. Des. 154 (2020) 21–46, https://doi.org/10.1016/j.cherd.2019.11.025.
[21] D. Huang, K. Men, D. Li, T. Wen, Z. Gong, B. Sunden, Z. Wu, Application of ultrasound technology in the drying of food products, Ultrason. Sonochem. 63 (2020), 104950.
[22] H.T. Sabarez, 14 - Airborne Ultrasound for Convective Drying Intensification, in: K. Knoerzer, P. Juliano, G.B.T.-I.F.P.T. Smithers (Eds.), Woodhead Publ. Ser. Food Sci. Technol. Nutr., Woodhead Publishing, 2016: pp. 361–386. 10.1016/B978-0-08-100294-0.00014-6.
[23] P. Li, Z. Chen, Experiment study on porous fiber drying enhancement with application of power ultrasound, Appl. Acoust. 127 (2017) 169–174, https://doi.org/10.1016/j.apacoust.2017.06.003.
[24] C. Peng, S. Ravi, V.K. Patel, A.M. Momen, S. Moghaddam, Physics of direct-contact ultrasonic cloth drying process, Energy. 125 (2017) 498–508.
[25] O. Kahraman, A. Malvandi, L. Vargas, H. Feng, Drying characteristics and quality attributes of apple slices dried by a non-thermal ultrasonic contact drying method, Ultrason. Sonochem. 73 (2021), 105510, https://doi.org/10.1016/j.ultsonch.2021.105510.
[26] A. Malvandi, H. Feng, M. Kamruzzaman, Application of NIR spectroscopy and multivariate analysis for Non-destructive evaluation of apple moisture content during ultrasonic drying, Spectrochim, Acta Part A Mol. Biomol. Spectrosc. 269 (2022), 120733, https://doi.org/10.1016/J.SAA.2021.120733.
[27] M. Prokic, Wideband multi-frequency, multimode, and modulated (MMM) ultrasonic technology BT - ultrasound technologies for food and bioprocessing, Springer New York, New York, NY, 2011, pp. 125–140, https://doi.org/10.1007/978-1-4419-7472-3_5.
[28] J.Y. Ahn, D.Y. Kil, C. Kong, B.G. Kim, Comparison of oven-drying methods for determination of moisture content in feed ingredients, Asian-Austral. J. Anim. Sci. 27 (2014) 1615–1622, https://doi.org/10.5713/ajas.2014.14305.
[29] D.S. Jayas, C.B. Singh, in: Drying of Agricultural Products BT - Encyclopedia of Agrophysics, Springer, Netherlands, Dordrecht, 2011, pp. 231–232, 10.1007/978-90-481-3585-1_44.
[30] J. Crank, The mathematics of diffusion, 2nd ed., Oxford University Press, 1979.
[31] A.S. Mujumdar, Handbook of Industrial Drying, 4th ed., CRC Press, Boca Raton, 2014 https://books.google.com/books?id=82_OBQAAQBAJ.
[32] P. Xu, A.P. Sasmito, A.S. Mujumdar, Heat and Mass Transfer in Drying of Porous Media, CRC Press, Boca Raton, 2019.
[33] M.U. Manual, Maplesoft, a division of Waterloo Maple Inc, (1996).
[34] P.C. Panchariya, D. Popovic, A.L. Sharma, Thin-layer modelling of black tea drying process, J. Food Eng. 52 (4) (2002) 349–357.
[35] G.E. Page, Factors influencing the maximum rates of air drying shelled corn in thin layers, Purdue University, 1949.
[36] S.M. Henderson, S. Pabis, Temperature effect on drying coefficient, J. Agric. Eng. Res. 6 (1961) 169–174.
[37] İ.T. Toğrul, D. Pehlivan, Mathematical modelling of solar drying of apricots in thin layers, J. Food Eng. 55 (3) (2002) 209–216.
[38] S.M. Henderson, Progress in developing the thin layer drying equation, Trans. ASAE. 17 (1974) 1167–1168.
[39] A. Midilli, H. Kucuk, Z. Yapar, A new model for single-layer drying, Dry. Technol. 20 (7) (2002) 1503–1513.
[40] C. Ertekin, M.Z. Firat, A comprehensive review of thin-layer drying models used in agricultural products, Crit. Rev. Food Sci. Nutr. 57 (2017) 701–717, https://doi.org/10.1080/10408398.2014.910493.
[41] J.J. Moré, The Levenberg-Marquardt algorithm: implementation and theory, in: Numer. Anal., Springer, 1978, pp. 105–116.
[42] R. Baini, T.A.G. Langrish, An assessment of the mechanisms for diffusion in the drying of bananas, J. Food Eng. 85 (2008) 201–214, https://doi.org/10.1016/j.jfoodeng.2007.06.035.
[43] C. Tunckal, İ. Doymaz, Performance analysis and mathematical modelling of banana slices in a heat pump drying system, Renew. Energy. 150 (2020) 918–923, https://doi.org/10.1016/j.renene.2020.01.040.
[44] F. Jensen, Activation energies and the Arrhenius equation, Qual. Reliab. Eng. Int. 1 (1) (1985) 13–17.
[45] A.R. Celma, F. Cuadros, F. López-Rodríguez, Convective drying characteristics of sludge from treatment plants in tomato processing industries, Food Bioprod. Process. 90 (2012) 224–234, https://doi.org/10.1016/j.fbp.2011.04.003.
[46] R.S. Hunter, R.W. Harold, The Measurement Of Appearance, John Wiley & Sons, 1987.

[47] A.M. Wolf, M.E. Watson, N. Wolf, Digestion and dissolution methods for P, K, Ca, Mg, and trace elements, in: Recomm. Methods Manure Anal., Madison, WI, USA, 2003: pp. 30–38.
[48] A.L.D. Goneli, P.C. Correa, M.A. Martins, Mathematical modeling of thin-layer drying kinetics of wheat, ASABE Pap. (2007).
[49] R. Bhadra, K.A. Rosentrater, K. Muthukumarappan, S. Kannadhason, Drying characteristics of distillers wet grains under varying condensed distillers solubles and drying temperature levels, Appl. Eng. Agric. 27 (2011) 777–786.
[50] M.R. Mosqueda, L.G. Tabil, Drying characteristics and lysine content of wheat distiller's grain with solubles under three drying methods, Dry. Technol. 29 (2011) 797–807, https://doi.org/10.1080/07373937.2010.540730.
[51] M. Zielinska, S. Cenkowski, M. Markowski, Superheated steam drying of distillers' spent grains on a single inert particle, Dry. Technol. 27 (2009) 1279–1285, https://doi.org/10.1080/07373930903195065.
[52] J.V. Santacatalina, M. Contreras, S. Simal, J.A. Cárcel, J.V. Garcia-Perez, Impact of applied ultrasonic power on the low temperature drying of apple, Ultrason. Sonochem. 28 (2016) 100–109, https://doi.org/10.1016/j.ultsonch.2015.06.027.
[53] K. A.r.p., K.E. Ileleji, R.L. Stroshine, Stress relaxation behavior of corn distillers dried grains with solubles (DDGS) in relation to caking, Powder Technol. 235 (2013) 866–872.
[54] A. v Luikov, Analytical Heat Diffusion Theory, Elsevier, 2012.
[55] C.A. Pickles, Drying kinetics of nickeliferous limonitic laterite ores, Miner. Eng. 16 (2003) 1327–1338, https://doi.org/10.1016/S0892-6875(03)00206-1.
[56] V.T. Karathanos, G. Villalobos, G.D. Saravacos, Comparison of two methods of estimation of the effective moisture diffusivity from drying data, J. Food Sci. 55 (1990) 218–223, https://doi.org/10.1111/j.1365-2621.1990.tb06056.x.
[57] P.B. Pathare, G.P. Sharma, Effective moisture diffusivity of onion slices undergoing infrared convective drying, Biosyst. Eng. 93 (2006) 285–291, https://doi.org/10.1016/j.biosystemseng.2005.12.010.
[58] A. Çağlar, İ.T. Toğrul, H. Toğrul, Moisture and thermal diffusivity of seedless grape under infrared drying, Food Bioprod. Process. 87 (2009) 292–300, https://doi.org/10.1016/j.fbp.2009.01.003.
[59] P.G. Debenedetti, Supercooled and glassy water, J. Phys. Condens. Matter. 15 (45) (2003) R1669–R1726.
[60] R. Baini, T.A.G. Langrish, Choosing an appropriate drying model for intermittent and continuous drying of bananas, J. Food Eng. 79 (2007) 330–343, https://doi.org/10.1016/j.jfoodeng.2006.01.068.
[61] G.L. Cromwell, K.L. Herkelman, T.S. Stahly, Physical, chemical, and nutritional characteristics of distillers dried grains with solubles for chicks and pigs, J. Anim. Sci. 71 (1993) 679–686, https://doi.org/10.2527/1993.713679x.
[62] V. Ganesan, K. Muthukumarappan, K.A. Rosentrater, Effect of moisture content and soluble level on the physical, chemical, and flow properties of distillers dried grains with solubles (DDGS), Cereal Chem. 85 (2008) 464–470, https://doi.org/10.1094/CCHEM-85-4-0464.
[63] I. Mavromichalis, The Maillard reaction in feed manufacturing, Feed Tech. 5 (2001) 13–14.
[64] J.M. Ames, Control of the Maillard reaction in food systems, Trends Food Sci. Technol. 1 (1990) 150–154.
[65] M.R.P. Mosqueda, Evaluation of Drying Technologies and Physico-Chemical Characterization of Wheat Distillers Dried Grain with Solubles (DDGS), Univ. Saskatchewan Saskatoon, SK, Canada, 2014.
[66] H. Gu, Y. Zhu, J. Li, Y. Peng, J. Huang, C. Bi, Ultrasound-assisted fractionation of dried distillers' grains with solubles (DDGS) at mild temperature for co-production of xylan and protein feed, J. Chem. Technol. Biotechnol. 94 (3) (2019) 829–836.
[67] T.W. Perry, A.E. Cullison, R.S. Lowrey, Feeds and Feeding, 6th ed., Pearson, London, 2002.
[68] C.M. Parsons, C. Martinez, V. Singh, S. Radhakrishman, S. Noll, Nutritional value of conventional and modified DDGS for poultry, in, Proc. Multi-State Poult. Nutr. Feed. Conf., Citeseer (2006).
[69] M. Umezawa, K. Sekita, K.-I. Suzuki, M. Kubo-Irie, R. Niki, T. Ihara, M. Sugamata, K. Takeda, Effect of aerosol particles generated by ultrasonic humidifiers on the lung in mouse, Part. Fibre Toxicol. 10 (2013) 64, https://doi.org/10.1186/1743-8977-10-64.